Least-squares RTM with wavefield decomposition

Mandy Wong

ABSTRACT

In least-squares reverse-time migration, the adjoint of the linearized forward-modeling operator suffers from back-scattering artifacts that severely hamper the speed of convergence. To avoid the back-scattering artifacts, I propose to use least-square reverse-time migration with wavefield decomposition. The incident and scattering wavefields are decomposed into up- and down-going direction such that only the forward-scattering component is used in imaging and modeling. Compared with using the conventional Laplacian preconditioning method, the proposed technique converges faster because it does not bias the inversion towards higher-frequency content. I demonstrate the concept and methodology with the 2D Seam model.

INTRODUCTION

It has been observed that the conventional cross-correlation imaging condition produces strong low-frequency migration artifacts in reverse-time migration (RTM) (Baysal et al., 1984). Migration artifacts appear mainly at shallow depth but also above strong reflectors. Figure 1 explains the generation of such artifacts. Due to the two-way propagation, source and receiver wavefields back-scatter off any hard velocity interfaces. With the cross-correlation imaging condition, the two-way propagation in RTM creates a wreath of possible imaging points. Figure 1 (a) and (b) show the location of undesirable cross-correlation energy that generate the low-frequency back-scattering artifacts. In least-squares reverse-time migration (LSRTM), the adjoint of the Born-modeling operator is equivalent to the RTM operator. LSRTM is considered to be a large problem that requires iterative inversion scheme. A successive sequence of adjoint and modeling operations is required to iteratively change the initial solution into the inverted one. As a result, when the adjoint operation is used in LSRTM, the back-scattering artifacts also exist in the gradient. Such artifacts hamper the convergence because erroneous energy in introduced into the gradient at every iterations.

There are many published work on how to suppress these artifacts (Baysal et al., 1984; Mulder and Plessix, 2003; Yoon et al., 2004; Fletcher et al., 2005). I will discuss two ways that can be incorporated into the LSRTM algorithm to suppress the back-scattering artifacts. A first way is to apply the Laplacian filter to the stacked RTM image. Zhang and Sun (2009) have showed that applying the Laplacian filter (along with a $1/\omega^2$ filter onto the data) is equivalent to applying a $cos^2\theta$ weight to the

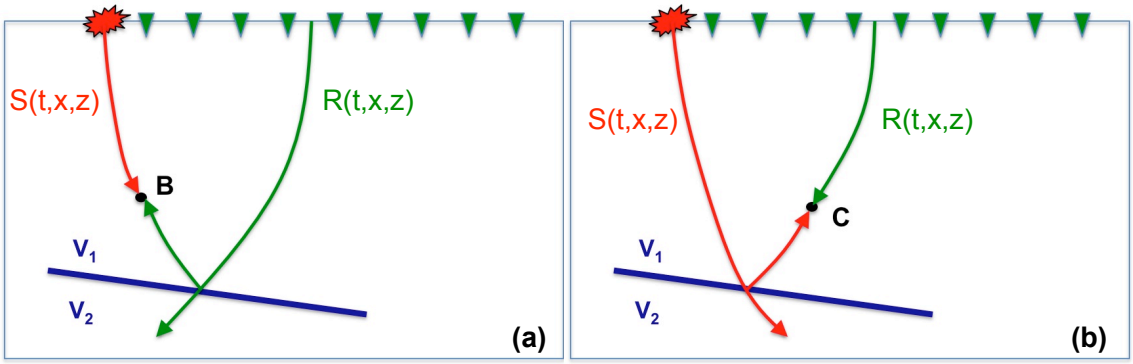

Figure 1: Consider an interaface with a sharp velocity contrast, migration artifacts occur when (a) the source wavefield correlate with the back-scattered receiver wavefield or (b) the vice-versa. [NR]

angle gather. This cosine factor down-weights contributions from large angle and effectively suppresses the back-scattered artifacts when $\theta = 90^o$. A straightforward incorporation of this idea in LSRTM is to use the Laplacian filter as a preconditioner in the inversion. The preconditioner scale low-frequency down to suppress the back-scattering artifact in the gradient.

The second approach to suppressing back-scattering artifacts is to decompose wavefields into one-way components and only cross-correlate the wave components that occur as reflections (Liu et al., 2007). However, fully decomposing wavefields into eight directions in 3D can be computationally expensive. Instead, I follow the ideas from Liu et al. (2011), which introduce an efficient algorithm for up-down decomposition of the source and receiver wavefields with having to save the entire wavefield in time. By decomposing the wavefields into up-going and down-going direction, the migration image (or the gradient) can be separated into forward and back-scattering components. Most of the RTM artifacts are contained in the back-scattering component, those noise can be conveniently excluded in the gradient calculation for LSRTM. While in the forward modeling direction of LSRTM, only the forward-scattering events will be calculated.

The paper starts with a discussion on the theory of LSRTM with wavefield decomposition. It will be followed by a comparison of some results between the Laplacian preconditioner and the wavefield decomposition approach of suppressing back-scattering artifact using a modified version of the 2D Seam model.

THEORY

Least-squares migration poses the imaging problem as an inversion problem by linearizing the wave equation with respect to our model ($m(\mathbf{x})$). The model is defined to be a weighted difference between the migration slowness ($s_o(\mathbf{x})$) and the true slowness

$(s(\mathbf{x}))$:

$$m(\mathbf{x}) = (s(\mathbf{x}) - s_o(\mathbf{x}))s_o(\mathbf{x}). \tag{1}$$

The constant-density acoustic isotropic wave-equation is used in this study. The wave-equation is linearized with respect to $m(\mathbf{x})$ by applying the first-order Born approximation. The forward-modeling equation is

$$d^{mod}(\mathbf{x_r}, \mathbf{x_s}, \omega) = \sum_{\mathbf{x}} \omega^2 f_s(\omega) G(\mathbf{x_s}, \mathbf{x}) m(\mathbf{x}) G(\mathbf{x}, \mathbf{x_r}). \tag{2}$$

where d^{mod} represents the forward modeled data, ω is the temporal frequency, $m(\mathbf{x})$ is a function of the image point $\mathbf{x}$, $f_s(\omega)$ is the source waveform, and $G(\mathbf{x_s}, \mathbf{x})$ is the Green's function of the two-way acoustic constant-density wave equation over the migration slowness. Note that G is actually ω-dependent and is a function of $s_o(\mathbf{x})$ only. The inversion problem is defined as minimizing the least-squares difference between the synthetic and the recorded data:

$$S(\mathbf{m}) = \| \mathbf{Lm} - \mathbf{d} \|^2 = \| \mathbf{d^{mod}} - \mathbf{d} \|^2, \tag{3}$$

where $\mathbf{L}$ is the matrix form of the forward-modeling operator as shown in equation 2. It is important to point out that the adjoint of the forward-modeling operator is the migration operator:

$$\begin{aligned} m_{mig}(\mathbf{x}) &= \sum_{\mathbf{x_r}, \mathbf{x_s}, \omega} \omega^2 f_s^*(\omega) G^*(\mathbf{x_s}, \mathbf{x}) G^*(\mathbf{x}, \mathbf{x_r}) d(\mathbf{x_r}, \mathbf{x_s}, \omega), \\ &= \sum_{\mathbf{x_s}, t} s(t, \mathbf{x}; \mathbf{x_s}) r(t, \mathbf{x}; \mathbf{x_s}). \end{aligned} \tag{4}$$

Note that the second line of equation 4 express the adjoint operation of the forward-modeling operation to the more familiar zero-lag cross-correlation imaging condition in RTM. $s(t, \mathbf{x})$ and $r(t, \mathbf{x})$ represent the source and receiver wavefield as a function of time t and sub-surface location $\mathbf{x}$. To reduce the back-scattering artifacts, Liu et al. (2011) propose to partition the source and receiver wavefields as

$$s(t, \mathbf{x}; \mathbf{x_s}) = s_d(t, \mathbf{x}; \mathbf{x_s}) + s_u(t, \mathbf{x}; \mathbf{x_s}), \tag{5}$$

and

$$r(t, \mathbf{x}; \mathbf{x_s}) = r_d(t, \mathbf{x}; \mathbf{x_s}) + r_u(t, \mathbf{x}; \mathbf{x_s}), \tag{6}$$

where $s_u(t, \mathbf{x}; \mathbf{x_s})$ and $s_d(t, \mathbf{x}; \mathbf{x_s})$ represents the up- and down-going partition of the source wavefield. Similarly, $r_u(t, \mathbf{x}; \mathbf{x_s})$ and $r_d(t, \mathbf{x}; \mathbf{x_s})$ represents the up- and down-going partition of the receiver wavefield. T is the recording time of the observed data. The imaging condition can then be decompose into four component by substituting

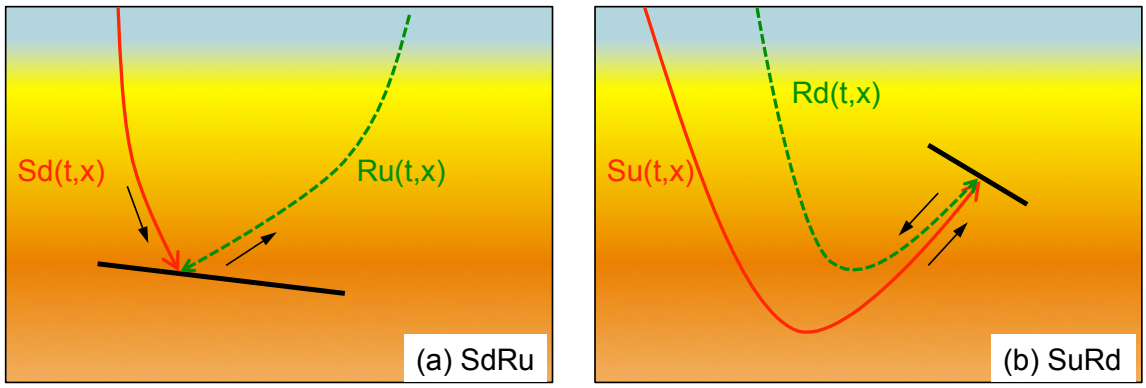

Figure 2: Ray-path diagrams of the imaging condition of (a) down-going source and up-going receiver wavefields and (b) up-going source and down-going receiver wavefields. These image points corresponds to the forward-scattering events. Note that the black arrows indicate the direction of wavefields when played forward in time. The green arrows indicate the direction of the receiver wavefields played in reverse time. [NR]

equation 5 and 6 into the imaging condition (equation 4).

$$
\begin{aligned}
m_{mig}(\mathbf{x}) &= I_1(\mathbf{x}) + I_2(\mathbf{x}) + I_3(\mathbf{x}) + I_4(\mathbf{x}), && (7)\\
I_1(\mathbf{x}) &= \sum_{\mathbf{x_s},t} s_d(t,\mathbf{x};\mathbf{x_s}) r_u(T-t,\mathbf{x};\mathbf{x_s}), && (8)\\
I_2(\mathbf{x}) &= \sum_{\mathbf{x_s},t} s_u(t,\mathbf{x};\mathbf{x_s}) r_d(T-t,\mathbf{x};\mathbf{x_s}), && (9)\\
I_3(\mathbf{x}) &= \sum_{\mathbf{x_s},t} s_u(t,\mathbf{x};\mathbf{x_s}) r_u(T-t,\mathbf{x};\mathbf{x_s}), && (10)\\
I_4(\mathbf{x}) &= \sum_{\mathbf{x_s},t} s_d(t,\mathbf{x};\mathbf{x_s}) r_d(T-t,\mathbf{x};\mathbf{x_s}), && (11)
\end{aligned}
$$

where $I_1(\mathbf{x})$ corresponds to the cross-correlation of the down-going source and up-going receiver wavefields as shown in Figure 2a . $I_2(\mathbf{x})$ corresponds to the cross-correlation of the up-going source and down-going receiver wavefields as shown in Figure 2b. Both terms produce images at reflection points. I will refer I_1 and I_2 as the forward-scattering term. On the other hand, $I_3(\mathbf{x})$ corresponds to the cross-correlation of the up-going source and up-going receiver wavefields while $I_4(\mathbf{x})$ corresponds to the cross-correlation of the down-going source and down-going receiver wavefields. These terms produce the low-frequency artifacts in RTM, illustrated by Figure 1. I will refer I_3 and I_4 as the back-scattering term. We can eliminate the back-scattering artifacts in the image with the following migration operator,

$$
m_{decomp}(\mathbf{x}) = \sum_{\mathbf{x_s},t} s_d(t,\mathbf{x};\mathbf{x_s}) r_u(t,\mathbf{x};\mathbf{x_s}) + s_u(t,\mathbf{x};\mathbf{x_s}) r_d(t,\mathbf{x};\mathbf{x_s}). \qquad (12)
$$

In general, extracting up- and down-going wavefield requires a 2D Fourier transform in (t, x_z) space. This is computationally expensive because the entire source and receiver wavefield must be saved in memory. To go around this problem, Liu et al. (2011) proposed decomposing the wavefields in the k_z axis, which only requires 1D Fourier transform in z. Let $\widetilde{s}(t, x, k_z)$ be the 1D Fourier transform of the source wavefield $s(t, \mathbf{x})$ in z. Let $s_+(t, \mathbf{x})$ and $s_-(t, \mathbf{x})$ represents the $k_z\pm$ decomposition of the source wavefield as,

$$\widetilde{s_+}(t, x, k_z) = \begin{cases} \widetilde{s}(t, x, k_z) & \text{if } \omega \geq 0 \\ 0 & \text{if } \omega < 0, \end{cases}$$

and

$$\widetilde{s_-}(t, x, k_z) = \begin{cases} 0 & \text{if } \omega \geq 0 \\ \widetilde{s}(t, x, k_z) & \text{if } \omega < 0, \end{cases}$$

where $\widetilde{s_+}(t, x, k_z)$ and $\widetilde{s_-}(t, x, k_z)$ is the 1D Fourier transform of a new representation of the decomposed source wavefields $s_+(t, \mathbf{x})$ and $s_-(t, \mathbf{x})$. Similar definition follows for the receiver wavefields $r_+(t, \mathbf{x})$ and $r_-(t, \mathbf{x})$. Liu et al. (2011) show that the imaging condition in equation 12 can also be written as

$$m_{decomp}(\mathbf{x}) = \sum_{\mathbf{x_s}, t} s_+(t, \mathbf{x}) r_-(t, \mathbf{x}) + s_-(t, \mathbf{x}) r_+(t, \mathbf{x}). \tag{13}$$

The forward-modeling direction is equivalent to the Born-modeling operator that corresponds to the forward-scattering events as illustrated in Figure 3a and b. A derivation of the forward-modeling operator using wavefields decomposition is shown in the appendix.

2D Seam model

I extracted a 2D velocity section of the Seam model for this study. Figure 4a shows the true velocity model used to generate synthetic data. The model is 16000 m wide, 7000 m deep and a spatial spacing of 20 m. 20 shots are evenly distributed at the surface. Each shot gather is generated with receivers located at every grid point at the surface. The migration velocity model (Figure 4b) is a smoothed version of the true velocity model in the sediment layers. I assume the salt is being picked correctly in the migration velocity model excluding the details of the dirty salt. Figure 4c shows the image model we wish to recover. The true model is calculated using equation 1.

I compare imaging result between RTM, LSRTM with Laplacian preconditioner, and LSRTM with wavefield decomposition. LSRTM with wavefield decomposition has been described in the previous section. In LSRTM with Laplacian preconditioner, a

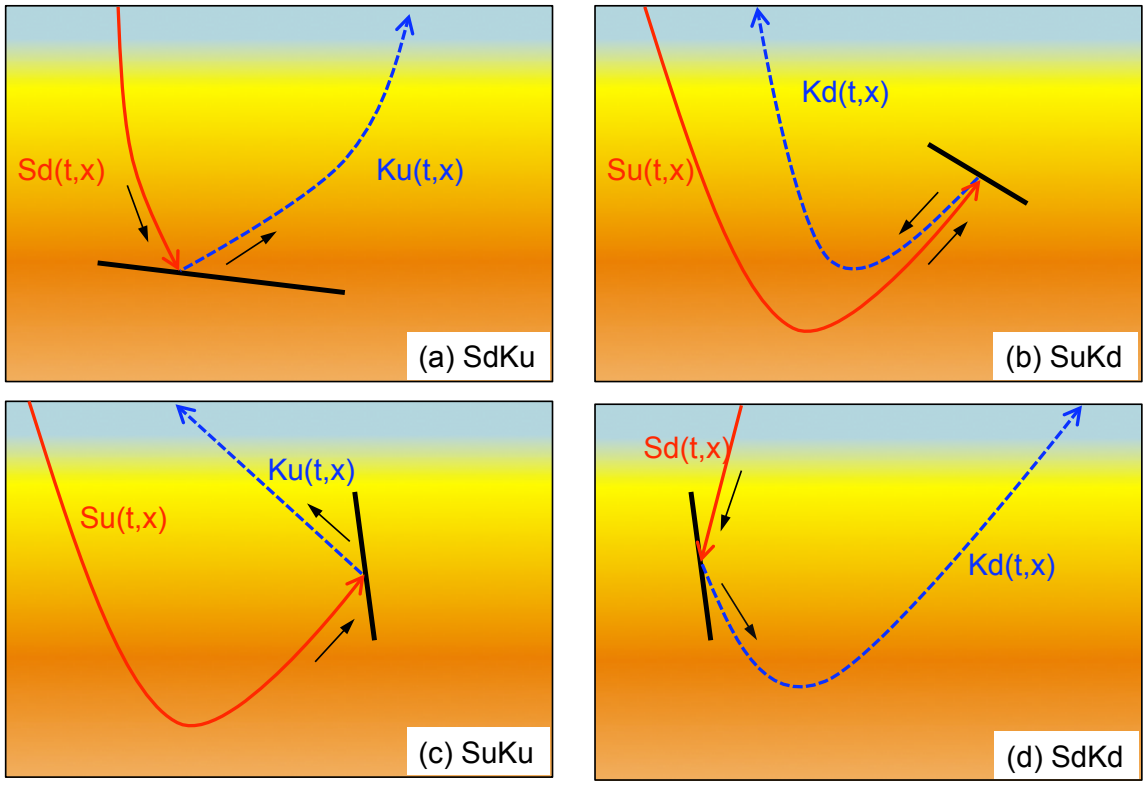

Figure 3: Ray-path diagram of the forward scattering events. (a) shows down-going incident ($s_d(t,\mathbf{x})$) and up-going scattered $k_u(t,\mathbf{x})$) wavefields and (b) up-going incident $s_u(t,\mathbf{x})$) and down-going $k_d(t,\mathbf{x})$) scattered wavefields. (c) and (d) show ray paths of some back-scattering events that are excluded from the migration and modeling. [NR]

new model variable $\mathbf{x}$ is defined such that $\mathbf{m} = \mathbf{A}\mathbf{x}$ where $\mathbf{A}$ is the Laplacian operator. Note that $\mathbf{A}$ is self-adjoint. Equation 3 then becomes

$$S(\mathbf{x}) = \| \mathbf{L}\mathbf{A}\mathbf{x} - \mathbf{d} \|^2 = \| \mathbf{d}^{\mathbf{mod}} - \mathbf{d} \|^2 . \tag{14}$$

Figure 5a shows the RTM image of the Seam model. In the RTM image, there are strong back-scattering artifacts above the salt layer that are suppressed with a Laplacian filter. When LSRTM with wavefield decomposition is applied, the gradient at every iteration is separated into the forward-scattering component (Figure 6a) and the back-scattering component (Figure 6b). Only the forward-scattering part is used to update the model. The sum of the forward- and back-scattering component (Figure 6) yields the gradient for regular LSRTM.

Figure 5b and 5c show the LSRTM image with the Laplacian preconditioning and with wavefield decomposition at iteration 20, respectively. In general, the LSRTM images are better than the RTM image (Figure 5a) with higher frequency content and better relative amplitude across the reflectors.

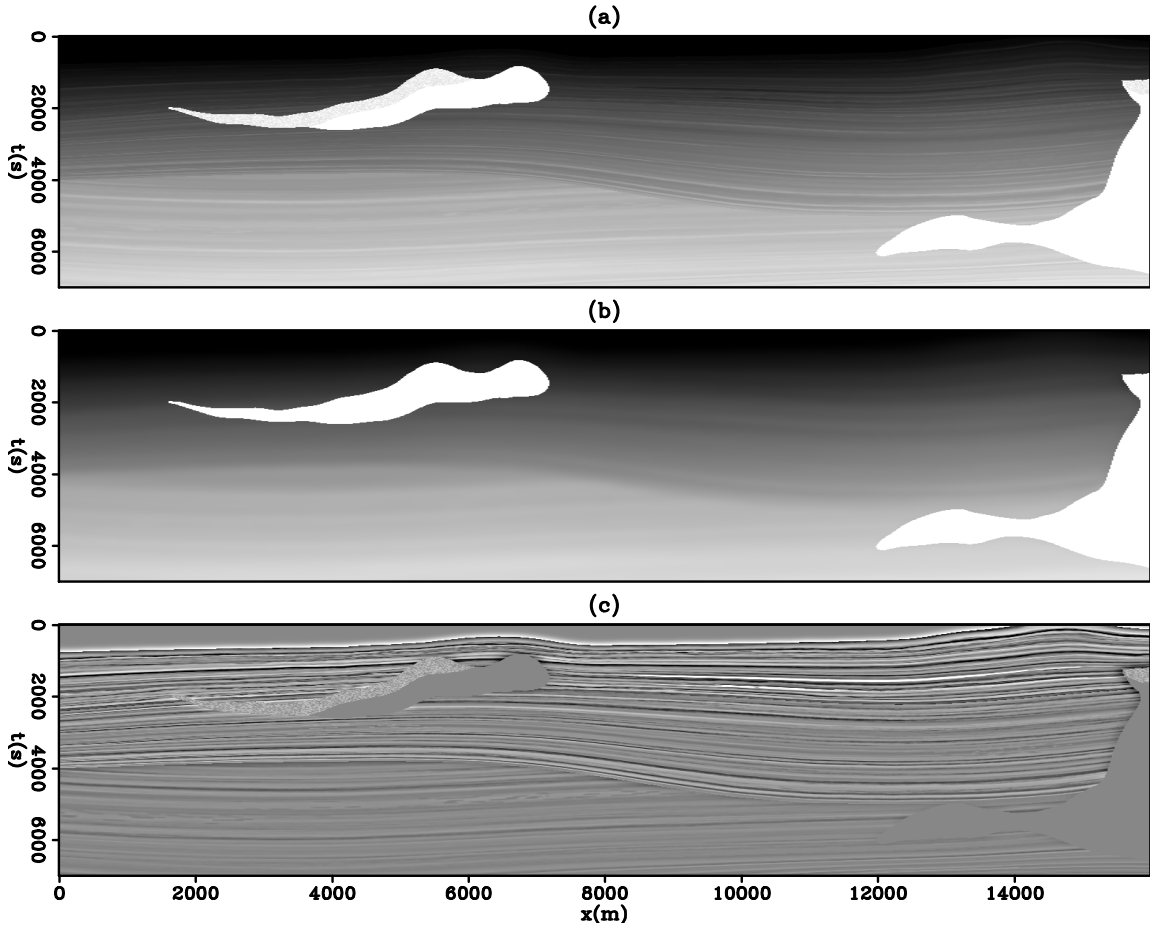

Figure 4: (a) True velocity, (b) migration velocity, and (c) true model. [ER]

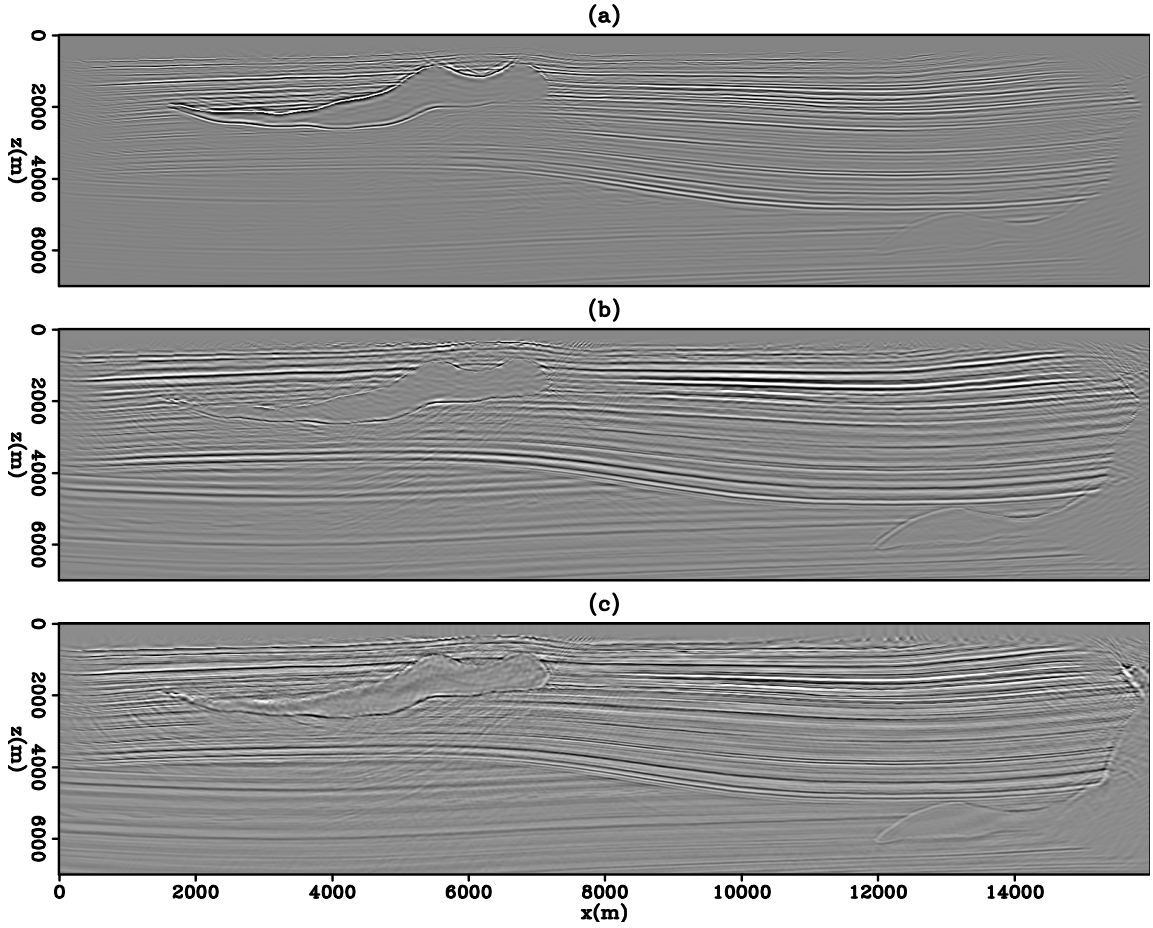

Figure 5: (a) RTM image, (b) LSRTM with Laplacian preconditioner at iteration 20, and (c) LSRTM with wavefield decomposition at iteration 20. [CR]

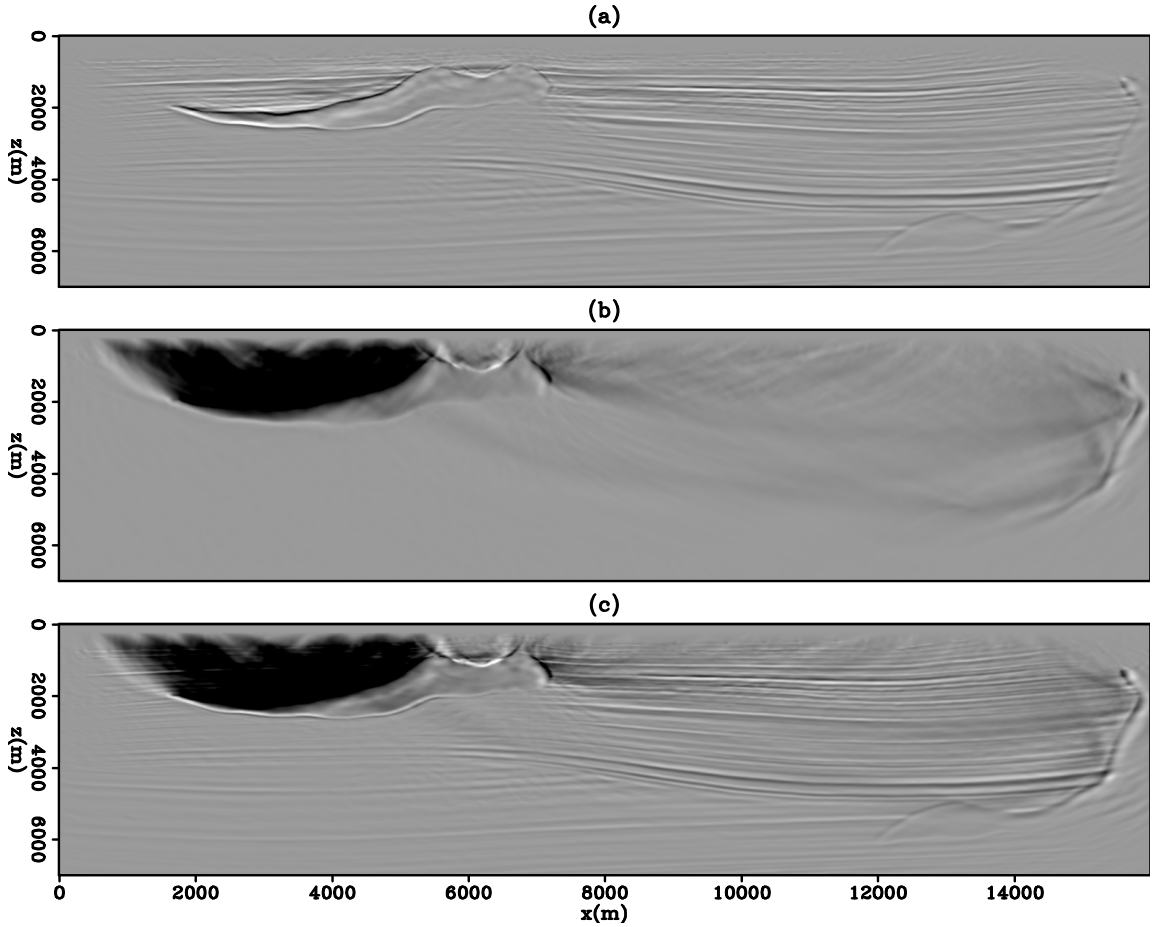

Figure 6: (a) Forward scattering part of the RTM image ($I_1 + I_2$), (b) back-scattering part of the migration image ($I_3 + I_4$) and (c) the total RTM image ($I_1 + I_2 + I_3 + I_4$). [CR]

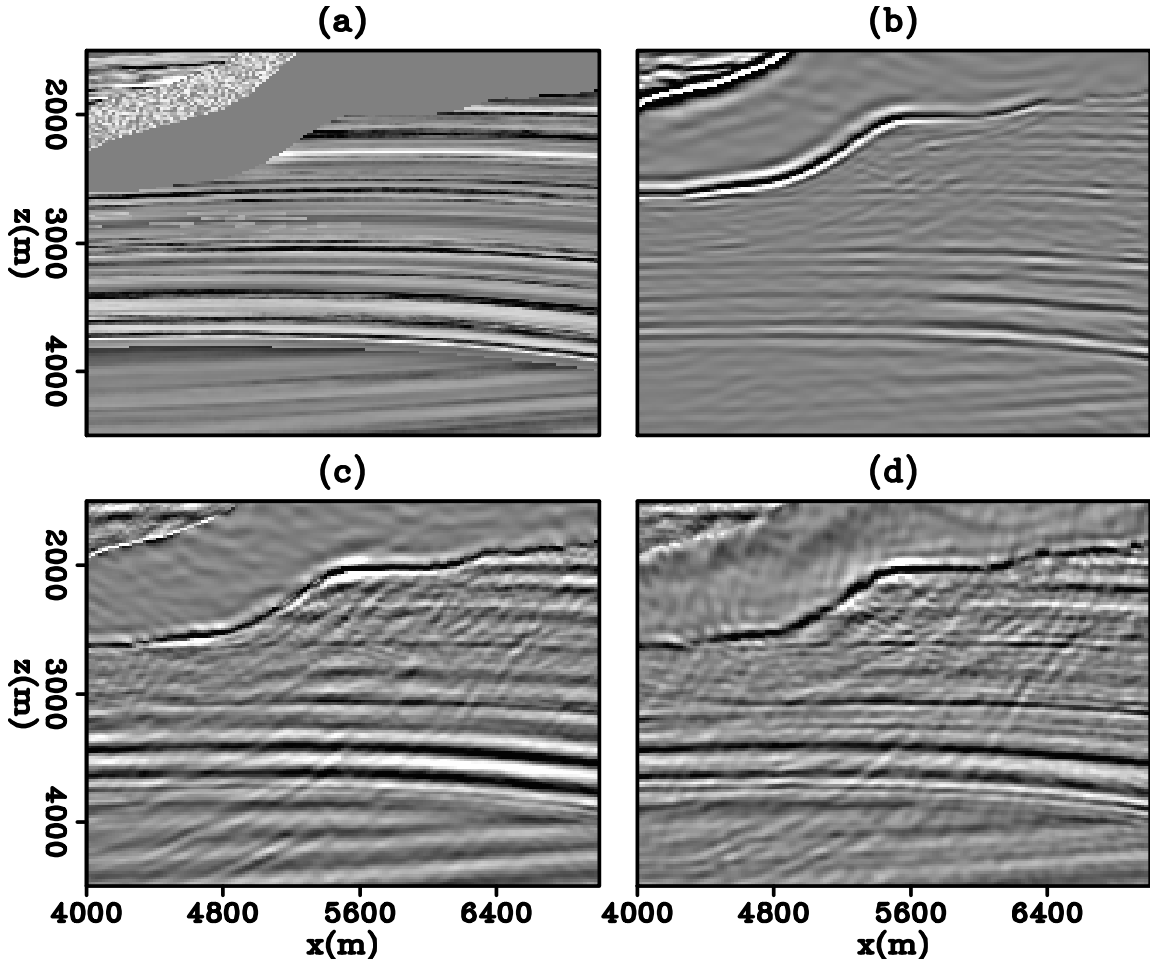

Figure 7: A zoomed section of (a) the true model, (b) RTM image, (c) LSRTM with Laplacian preconditioner, and (d) LSRTM with wavefield decomposition. [CR]

To compare between the two LSRTM results, let look at two zoomed areas. Figure 7 shows a zoomed section of the image from $x = 4000 - 7200m$ and $z = 1500 - 4500m$. We can easily identify the shadow zone underneath the salt structure in the RTM image (Figure 7b). The information in the shadow zone is partially recovered with LSRTM as shown in Figure 7c and d. The quality of the inverted image can be evaluated by looking at the relative strength of the reflectors across the image. By comparing the relative amplitude with the true model (Figure 7a), the LSRTM image with wavefield decomposition (Figure 7d) has better relatively amplitude information than the LSRTM image with Laplacian preconditioner (Figure 7c). Figure 9 shows the convergence curve between the two inversion. One remark is that using wavefield decomposition seems to allow the inversion to converge faster than using the Laplacian preconditioner. At iteration 10, the residual in wavefield decomposition has dropped down to below 5% while the residual from the Laplacian preconditioner is at around 10%.

Figure 8 shows another zoomed section of the image from $x = 7000 - 10000m$ and $z = 3500 - 6000m$. Figure 8a is the true model we wish to recover. Figure 8b is the RTM image. Notice that some of the higher frequency structures as annotated by circles is not well represented in the RTM image. Those structures are better represented in Figure 8 c, d, e, and f with LSRTM. By comparing both result at iteration 10, the Laplacian preconditioning image (Figure 8c) is less refined than the wavefield decomposition image (Figure 8d). However, as the inversion progress to iteration 40, the Laplacian preconditioning result (Figure 8e) has recovered some refined details. The images from iteration 10 and 40 suggests that LSRTM with wavefield decomposition converges faster than with Laplacian preconditioner.

DISCUSSIONS

Amplitude bias

From the synthetic result, I observe that LSRTM with wavefield decomposition converges faster than LSRTM with the Laplacian preconditioner. One explanation is because the later method tends to bias the inversion towards fitting the higher frequency. Figure 10 shows the amplitude spectrum of one shot gather from the input data and from the forward modeling of the first gradient from the two LSRTM methods. The spectrum is calculated by taking Fourier transform in time of each trace in the shot gather and the resulting spectrum is average along all traces (receivers) in the shot gather. Notice that the spectrum from the wavefield decomposition technique is much closer to the spectrum of the input data than that of the Laplacian preconditioning. The frequency bias can be compensated by adding a left-preconditioner in the inversion with the following fitting goal:

$$\mathbf{P}(\mathbf{LAx} - \mathbf{d^{obs}}) \approx 0, \tag{15}$$

where $\mathbf{P}$ represents the $\frac{1}{\omega^2}$ filter. However, the affects of including a left-preconditioner along with other data-weighting term will need to be studied.

Including the back-scattering term

One drawback for using LSRTM with wavefield decomposition is that some true back-scattering event (Figure 3c and d) will be excluded from the inversion. This implies that some steeply dipping reflectors might not be imaged with this technique. One way to address this problem is to introduce a spatially varying weighting for the back-scattering term.

$$m_{mig}(\mathbf{x}) = I_1(\mathbf{x}) + I_2(\mathbf{x}) + M_{back}(\mathbf{x})(I_3(\mathbf{x}) + I_4(\mathbf{x})), \tag{16}$$

where $M_{back}(\mathbf{x})$ is a image-space weighting function. It is set to zero for regions with strong back-scattering artifacts and is set to ones elsewhere. The region with strong

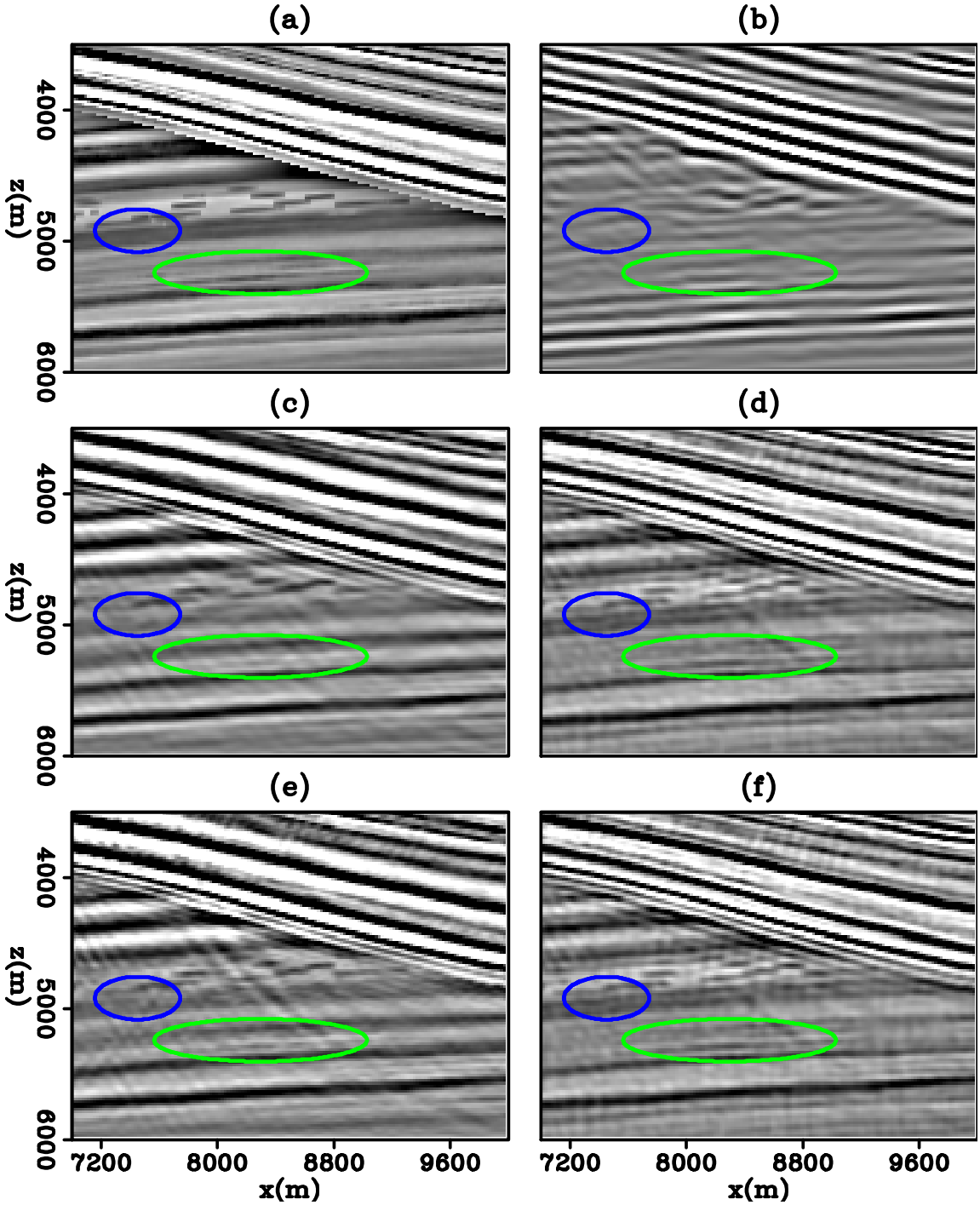

Figure 8: A zoomed section of (a) the true model, (b) RTM image, (c) LSRTM with Laplacian preconditioner at iteration 10, (d) LSRTM with wavefield decomposition at iteration 10, (e) LSRTM with Laplacian preconditioner at iteration 40 and (f) LSRTM with wavefield decomposition at iteration 40. All images are scaled to one and are displayed at the same clip of ± 0.25. [CR]

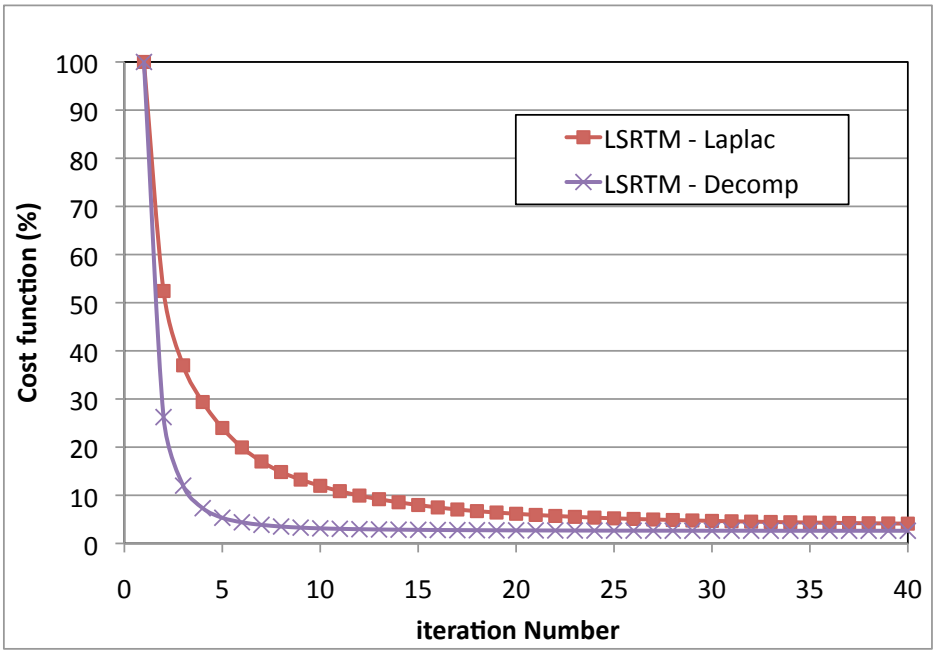

Figure 9: Convergence plot for LSRTM with the Laplacian preconditioner (square marker) and LSRTM with wavefield decomposition (cross marker). In general, using wavefield decomposition converges faster than using Laplacian preconditioner. [NR]

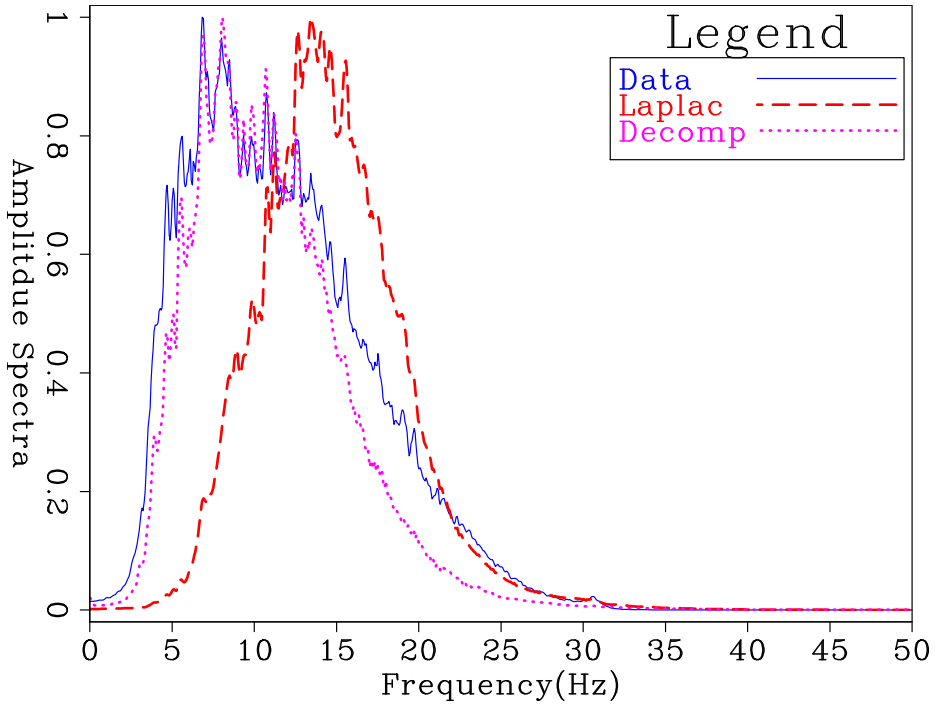

Figure 10: Amplitude spectrum of one shot gather from the input data (solid line). The amplitude spectrum of the forward modeling of the first gradient from LSRTM with Laplacian preconditioner (dash line) and LSRTM with wavefield decomposition (dotted line). [CR]

back-scattering artifacts is generally in the shallow region. This weighting would at least allow some true back-scattering event to be included in the inversion. Further study will be needed for this approach.

CONCLUSION

Back-scattering artifacts in reverse-time migration occur when diving waves, head waves or backscattered waves cross-correlate. These events are particularly strong where high velocity contrasts exist. In LSRTM, the adjoint of the linearized forward-modeling operator suffers from back-scattering artifacts that severely hamper the speed of convergence. One solution to this problem is to use a Laplacian filter as a preconditioner, which suppress lower-frequency and boost up higher-frequency. An alternate approach is to use LSRTM with wavefield decomposition. Based on the 2D Seam example, I found that the proposed technique allow the inversion to converge faster than using LSRTM with the Laplacian preconditioner.

ACKNOWLEDGMENTS

I thank Kittinat Taweesintananon for previous work on this topic. I also thank Biondo Biondi and Shuki Ronen for helpful discussion.

REFERENCES

Baysal, E., D. Kosloff, and J. Sherwood, 1984, A two-way nonreflecting wave equation: Geophysics, **49**, 131–141.

Fletcher, R., P. Fowler, P. Kitchenside, and U. Albertin, 2005, Suppressing artifacts in presetack reverse time migration: SEG Expanded Abstracts, 2049–2051.

Liu, F., G. Zhang, S. Morton, and J. Leveille, 2007, Reverse-time migration using one-way wavefield imaging condition: SEG Expanded Abstracts, **76**, S29–S39.

———, 2011, Reverse-time migration using one-way wavefield imaging condition: Geophysics, 2170–2174.

Mulder, W. and R.-E. Plessix, 2003, One-way and two-way wave equation migration: SEG Expanded Abstracts, 881–884.

Yoon, K., K. Marfurt, and W. Starr, 2004, Challenges in reverse-time migration: SEG Expanded Abstracts, 1057–1060.

Zhang, Y. and J. Sun, 2009, Practical issues in reverse time migration: true amplitude gathers, noise removal and harmonic source encoding: First break, **26**, 30–35.

APPENDIX

Forward modeling with wavefield decomposition

The goal here is to show that the adjoint of equation 12 is the Born-modeling equivalent of the forward scattering events. The derivation will be shown in 2D but extension to 3D is straight forward. To simplify notation, I will represent the model $m(x,z)$ and the data $d(x_r,t)$ as matrices $\mathbf{M}$ and $\mathbf{D_r}$ of dimension (x,z,t). The relationship is summarized as follow,

$$m(x,z) = \sum_t \mathbf{M}(x,z,t) = \mathbf{AM}, \tag{17}$$

$$\mathbf{D_r}(x,z,t) = \mathbf{L}_r d(x_r, z=0, t), \tag{18}$$

where matrix $\mathbf{A}$ is a stacking along the time axis t and $\mathbf{L}_r$ project the data at receiver location x_r. Let think of the input and output of the modeling and migration operators as M and D_r. The decomposing migration operator of equation 12 can be re-written in matrix form as follow,

$$\mathbf{M} = \mathbf{S_u K_d G D_r} + \mathbf{S_d K_u G D_r}. \tag{19}$$

In the above equation, $\mathbf{S_u}$ and $\mathbf{S_d}$ are up- and down-going source wavefield, respectively. $\mathbf{G}$ is the matrix operator form of the Green's function. $\mathbf{K_u}$ and $\mathbf{K_d}$ decomposition operators that partition wavefields into up- and down-going direction. They are defined as,

$$\mathbf{K_u} = \mathbf{F^{-1}}\widetilde{\mathbf{k_u}}\mathbf{F}, \tag{20}$$

$$\mathbf{K_d} = \mathbf{F^{-1}}\widetilde{\mathbf{k_d}}\mathbf{F}, \tag{21}$$

where F and F^{-1} is the forward and inverse 2D Fourier transform in (z,t). $\widetilde{\mathbf{k_u}}$ and $\widetilde{\mathbf{k_d}}$ extract up- and down-going direction in the (k_z,ω) space;

$$\widetilde{\mathbf{k_u}} = \begin{cases} 1 & \text{if } \omega k_z \geq 0 \\ 0 & \text{if } \omega k_z < 0, \end{cases}$$

$$\widetilde{\mathbf{k_d}} = \begin{cases} 0 & \text{if } \omega k_z \geq 0 \\ 1 & \text{if } \omega k_z < 0. \end{cases}$$

Note that the decomposition operators are self-adjoint. The forward-modeling operator with wavefield decomposition is defined to be

$$\mathbf{D_r} = \mathbf{G^* K_u^* S_d^* M} + \mathbf{G^* K_d^* S_u^* M}. \tag{22}$$

In the first term of equation 22, down-going source wavefield is multiplied with model $\mathbf{M}$ and only the up-going component is extracted by the operator $\mathbf{K_u}$. The extracted energy then propagates back to the receiver by $\mathbf{G}^*$. In the second term, the up-going source wavefield multiplies the model $\mathbf{M}$ and only the down-going component is extracted.

Forward modeling with up-down and $k_z\pm$ decomposition

The goal of this section is to show that the forward-modeling with up-down decomposition can also be represented with the $k_z\pm$ representation. This section follows the prove similar to that in the paper Liu et al. (2011) for the migration direction. Let first re-write equation 22 with an explicit dependence on the variable ω

$$\widetilde{\mathbf{d_r}}(\omega) = \widetilde{\mathbf{g}}^*(\widetilde{\mathbf{k_u^*}}(\omega)\widetilde{\mathbf{s}}^*_{\mathbf{d}}(\omega) + \widetilde{\mathbf{g}}^*\widetilde{\mathbf{k}}^*_{\mathbf{d}}(\omega)\widetilde{\mathbf{s}}^*_{\mathbf{u}}(\omega))\widetilde{\mathbf{m}}. \tag{23}$$

The up-down decomposition can be expressed in terms of the $k_z\pm$ wavefields in the following ways:

$$\widetilde{\mathbf{k_u}}(\omega) = \begin{cases} \widetilde{\mathbf{k}_+}(\omega) & \text{if } \omega \geq 0 \\ \widetilde{\mathbf{k}_-}(\omega) & \text{if } \omega < 0, \end{cases}$$

$$\widetilde{\mathbf{k_d}}(\omega) = \begin{cases} \widetilde{\mathbf{k}_-}(\omega) & \text{if } \omega \geq 0 \\ \widetilde{\mathbf{k}_+}(\omega) & \text{if } \omega < 0, \end{cases}$$

$$\widetilde{\mathbf{s_u}}(\omega) = \begin{cases} \widetilde{\mathbf{s}_+}(\omega) & \text{if } \omega \geq 0 \\ \widetilde{\mathbf{s}_-}(\omega) & \text{if } \omega < 0, \end{cases}$$

and

$$\widetilde{\mathbf{s_d}}(\omega) = \begin{cases} \widetilde{\mathbf{s}_-}(\omega) & \text{if } \omega \geq 0 \\ \widetilde{\mathbf{s}_+}(\omega) & \text{if } \omega < 0. \end{cases}$$

The $\widetilde{\mathbf{k}_\pm}(\omega)$ are the $\widetilde{\mathbf{k}}(\omega)$ wavefield with $k_z\pm$ decomposition as referenced in Liu et al. (2011). Substituting the above equations into equation 23 gives

$$\widetilde{\mathbf{d_r}}(\omega) = \begin{cases} \widetilde{\mathbf{g}}^*(\widetilde{\mathbf{k}^*_+}\widetilde{\mathbf{s}^*_-} + \widetilde{\mathbf{k}^*_-}\widetilde{\mathbf{s}^*_+})\widetilde{\mathbf{m}} & \text{if } \omega \geq 0 \\ \widetilde{\mathbf{g}}^*(\widetilde{\mathbf{k}^*_-}\widetilde{\mathbf{s}^*_+} + \widetilde{\mathbf{k}^*_+}\widetilde{\mathbf{s}^*_-})\widetilde{\mathbf{m}} & \text{if } \omega < 0, \end{cases}$$

which shows that the forward modeling with up-down decomposition (equation 23) is equivalent to the forward-modeling with $k_z\pm$ decomposition.

$$\widetilde{\mathbf{d_r}}(\omega) = \widetilde{\mathbf{g}}^*(\widetilde{\mathbf{k}^*_+}(\omega)\widetilde{\mathbf{s}^*_-}(\omega) + \widetilde{\mathbf{g}}^*\widetilde{\mathbf{k}^*_-}(\omega)\widetilde{\mathbf{s}^*_+}(\omega))\widetilde{\mathbf{m}}. \tag{24}$$